Chapter 15
Discrete Nonlinear Schrödinger Equations with Time-Dependent Coefficients (*Management* of Lattice Solitons)

Jesús Cuevas and Boris A. Malomed

15.1 Introduction

The general topic of the book into which this chapter is incorporated is the discrete nonlinear Schrödinger (DNLS) equation as a fundamental model of nonlinear lattice dynamics. The DNLS equation helps to study many generic features of nonintegrable dynamics in discrete media [1]. Besides being a profoundly important model in its own right, this equation has very important direct physical realizations, in terms of arrays of nonlinear optical waveguides (as was predicted long ago [2] and demonstrated in detail more recently, see [3, 4] and references therein), and arrays of droplets in Bose–Einstein condensates (BECs) trapped in a very deep optical lattice (OL), see details in the original works [5–10] and the review [11].

In all these contexts, discrete solitons are fundamental localized excitations supported by the DNLS equation. As explained in great detail in the rest of the book, the dynamics of standing solitons, which are pinned by the underlying lattice, is understood quite well, by means of numerical methods and analytical approximations (the most general approximation is based on the variational method [12, 13]). A more complex issue is posed by moving discrete solitons [14–17]. While, strictly speaking, exact solutions for moving solitons cannot exist in nonintegrable lattice models because of the radiation loss, which accompanies their motion across the lattice, direct simulations indicate that a soliton may move freely if its norm ("mass") does not exceed a certain critical value [17]. In the quasi-continuum approximation, the moving soliton may be considered, in the lowest (adiabatic) approximation, as a classical mechanical particle which moves across the effective Peierls–Nabarro (PN) potential induced by the lattice [18–21]. In this limit, the radiation loss is a very weak nonadiabatic effect, which attests to the deviation of the true soliton dynamics from that of the point-like particle.

In the case of the DNLS equation describing arrays of nearly isolated droplets of a BEC trapped in a deep OL, an interesting possibility is to apply the *Feshbach*

J. Cuevas (✉)
Grupo de Física No Lineal, Departamento de Física Aplicada I, Escuela Universitaria Politécnica, C/ Virgen de África, 7, 41011 Sevilla, Spain
e-mail: jcuevas@us.es

P.G. Kevrekidis, *The Discrete Nonlinear Schrödinger Equation*, STMP 232, 277–291, DOI 10.1007/978-3-540-89199-4_15,

resonance management (FRM) to this system, as was first proposed and studied for immobile discrete solitons in [22], and later elaborated in detail, for moving solitons, in [23]. The FRM may be induced by an external low-frequency ac magnetic field, which periodically (in time) changes the sign of the nonlinearity by dint of the FRM, i.e., formation of quasi-bound states in collisions between atoms [24]. For the effectively one-dimensional BEC in the absence of the OL, the concept of the FRM was elaborated in (1D) [25], see also the book [26].

The objective of the chapter is to summarize basic results for the quiescent and moving 1D DNLS solitons subjected to the time-periodic management, following, chiefly, the lines of works [22] and [23]. For the quiescent solitons, most significant findings are FRM-induced resonances in them, and stability limits for the solitons which are affected by the resonant mechanisms. In particular, resonances with an external time-periodic modulation may stimulate self-splitting of the solitons. For the moving solitons, an essential conclusion is that the FRM may strongly facilitate their mobility, which is an essentially novel dynamical effect in discrete media.

The DNLS equation which includes the FRM mechanism can be cast in the following form:

$$i\dot{u}_n + C\,(u_{n+1} + u_{n-1} - 2u_n) + g(t)|u_n|^2 u_n = 0, \tag{15.1}$$

where $u_n(t)$ denotes the BEC wave function at the lattice sites, C is the strength of the linear coupling between adjacent sites of the lattice, and the real time-dependent nonlinear coefficient is

$$g(t) = g_{\rm dc} + g_{\rm ac}\sin(\omega t) \tag{15.2}$$

with the time-dependent term accounting for the FRM ($-g$ is proportional to the scattering length of atomic collisions, whose magnitude and sign may be directly altered by the FRM). In what follows below, we fix, by means of obvious rescaling, $C \equiv 1$. We also note that $g_{\rm dc}$ may always be chosen positive, as it can be transformed by means of the so-called staggering transformation, $u_n(t) \equiv (-1)^n e^{-4it}\tilde{u}_n(t)$. Equation (15.1) with the time-dependent nonlinear coefficient has a single dynamical invariant, the norm (which is proportional to the number of atoms in the BEC),

$$\mathcal{N} = \sum_{n=-\infty}^{+\infty} |u_n|^2. \tag{15.3}$$

The chapter is divided into two major parts that deal with quiescent and mobile discrete solitons (the latter one also briefly considers collisions between the moving solitons). Each part contains sections which present analytical and numerical results. In either case, the analytical approach is based on using a particular *ansatz* for the shape of the soliton, while numerical results are produced by systematic direct simulations of Eq. (15.1) with appropriate initial conditions.

15.2 Quiescent Solitons Under the Action of the "Management"

15.2.1 Semi-Analytical Approximation

In this section, we put Eqs. (15.1) and (15.2) in a slightly different form, namely,

$$i\dot{u}_n + \frac{1}{2}\left(u_{n+1} + u_{n-1} - 2u_n\right) + a(t)\left|u_n\right|^2 u_n = 0,\ a(t) = 1 + a_1 \sin\left(\omega t\right), \quad (15.4)$$

where, as said above, we fix $C = 1$, and the dc part of $a(t)$ is also set equal to 1 by means of an additional rescaling. A (semi-)analytical approximation for soliton solutions to Eq. (15.4) is based on the fact that it can be derived from the Lagrangian,

$$L = \frac{1}{2}\sum_{n=-\infty}^{\infty}\left[i\left(u_n^*\dot{u}_n - u_n\dot{u}_n^*\right) - \left|u_{n+1} - u_n\right|^2 + a(t)|u_n|^4\right] \quad (15.5)$$

(* stands for the complex conjugate). Then, the variational approximation (VA) [13] represents the solitons by the following *ansatz*, following [12]:

$$u_n(t) = A\exp(i\phi + ib|n| - \alpha|n|), \quad (15.6)$$

where A, ϕ, b, and α are real functions of time. Substituting this ansatz in the Lagrangian (15.5), it is easy to perform the summations explicitly and thus arrive at the corresponding *effective Lagrangian* (an inessential term, proportional to $\dot{\phi}$, is dropped here):

$$\frac{L}{\mathcal{N}} = -\frac{1}{\sinh\left(2\alpha\right)}\frac{db}{dt} + \frac{\cos b}{\cosh\alpha} + \frac{1}{4}\mathcal{N}a(t)\frac{\sinh\alpha}{\cosh^3\alpha}\cosh\left(2\alpha\right), \quad (15.7)$$

where $\mathcal{N} = A^2\coth\alpha$ is the norm of the ansatz (recall the norm is the dynamical invariant, calculated as per Eq. (15.3)). The variational equations for the soliton's *chirp* b and inverse width α, derived from Lagrangian (15.7) are

$$\frac{db}{dt} = 2\left(\cos b\right)\frac{\sinh^3\alpha}{\cosh\left(2\alpha\right)} - \frac{1}{2}\mathcal{N}a(t)\left(\tanh^2\alpha\right)\frac{2\cosh\left(2\alpha\right) - 1}{\cosh\left(2\alpha\right)}, \quad (15.8)$$

$$\frac{d\alpha}{dt} = -\left(\sin b\right)\left(\sinh\alpha\right)\tanh\left(2\alpha\right) \quad (15.9)$$

(the amplitude A was eliminated here in favor of α, due to the conservation of $\mathcal{N}$). First, in the absence of the FRM, i.e., for $a(t) = \text{const} \equiv 1$ (see Eq. (15.4)) Eqs. (15.8) and (15.9) give rise to a stationary solution (*fixed point*, FP), with $b_{\text{FP}} = 0$ and α_{FP} defined by equation $\sinh\left(\alpha_{\text{FP}}\right) = \mathcal{N}\left[1 + 3\tanh^2\left(\alpha_{\text{FP}}\right)\right]/4$ [12]. The VA-predicted stationary soliton is quite close to its counterpart found from a numerical solution of Eq. (15.4) with $a(t) \equiv 1$ [22]. Furthermore, linearization of

Eqs. (15.8) and (15.9) around the FP yields a squared frequency of intrinsic oscillations for a slightly perturbed soliton,

$$\omega_0^2 = \frac{\sinh^3(\alpha_{\rm FP})\cosh^2(\alpha_{\rm FP})}{\cosh^3(2\alpha_{\rm FP})}\left\{4\sinh(\alpha_{\rm FP})[\cosh(2\alpha_{\rm FP})+2] - \frac{\mathcal{N}}{\cosh^4(\alpha_{\rm FP})}\left[5\cosh^2(2\alpha_{\rm FP}) - 2\cosh(2\alpha_{\rm FP}) - 1\right]\right\} \tag{15.10}$$

(this expression can be shown to be always positive). Comparison of this prediction of the VA with numerically found frequencies of small oscillations of the perturbed soliton demonstrates good agreement too [22].

In the presence of the FRM, $a_1 \neq 0$, strong (resonant) response of the system is expected when the modulation frequency ω is close to eigenfrequency given by Eq. (15.10). Moreover, the dynamics may become chaotic, via the resonance-overlapping mechanism [27], if the modulation amplitude a_1 exceeds some threshold value. This was observed indeed in numerical simulations of Eqs. (15.8) and (15.9), as illustrated in Fig. 15.1 by a typical example of the Poincaré map [27] in the chaotic regime. The figure shows discrete trajectories initiated by two sets of the initial conditions, namely, $\left(b_0^{(1)}, \alpha_0^{(1)}\right) = (0, 0.789)$, that correspond to the stationary discrete soliton with amplitude $A = 1$ (cf. ansatz (15.6)) in the unperturbed system ($a_1 = 0$), and a different set, $\left(b_0^{(2)}, \alpha_0^{(2)}\right) = (0.13, 0.74)$. The respective modulation frequency, ω, is close to the eigenfrequency of small oscillations ω_0, as predicted by Eq. (15.10). For the former initial condition, the point in space (b, α) is chaotically moving away from the unperturbed FP. However, the chaotic evolution is a *transient feature*, as the discrete trajectory takes an asymptotic form with $\alpha(t) \to 0$, which implies decay (indefinite broadening) of the soliton. The second set of the initial conditions eventually leads to a *stable periodic solution* (in terms of the Poincaré map, it is represented by a new FP, which is found in a vicinity of the unperturbed one). The latter results predicts the existence of quasi-stationary discrete solitons under the action of the FRM.

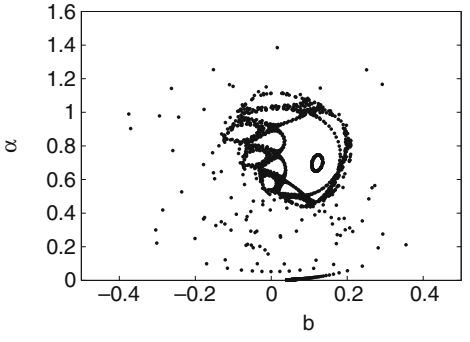

Fig. 15.1 Example of the chaotic Poincaré map generated by Eqs. (15.8) and (15.9) with $a_1 = 0.02766$, $\omega = 0.481$, and $W = 1.5202$. Reprinted from [22] with permission

Another analytically tractable case is one for the high-frequency modulation. It is then possible to perform averaging of Eq. (15.4) (without resorting to the VA). The eventual result is an effective DNLS equation for the slowly varying part of the lattice field, $q_n(t)$ [22]:

$$
\begin{aligned}
& i\dot{q}_n + \frac{1}{2}(q_{n+1} + q_{n-1} - 2q_n) + |q_n|^2 q_n \\
& = \left(a_1^2/8\omega^2\right)\left[3|q_n|^4 (q_{n+1} + q_{n-1}) + 2|q_n|^2 q_n^2 \left(q_{n+1}^* + q_{n-1}^*\right)\right. \\
& \quad + |q_{n+1}|^4 q_{n+1} + |q_{n-1}|^4 q_{n-1} - 2|q_{n+1}|^2 \left(2|q_n|^2 q_{n+1} + q_n^2 q_{n+1}^*\right) \\
& \quad \left. - 2|q_{n-1}|^2 \left(2|q_n|^2 q_{n-1} + q_n^2 q_{n-1}^*\right)\right]. \qquad (15.11)
\end{aligned}
$$

Equation (15.11) is the DNLS equation with a small inter-site quintic perturbation ($a_1^2/8\omega^2$ is a small perturbation parameter).

15.2.2 Direct Simulations

Systematic direct simulations of Eq. (15.4) demonstrate that the VA correctly predicts only an initial stage of the dynamics [22]. Emission of linear waves (lattice phonons) by the soliton, which is ignored by the VA, gives rise to an effective dissipation, that makes the resonance frequency different from the value predicted by Eq. (15.10). Actually, the soliton decouples from the resonance, as ω_0 depends on the norm $\mathcal{N}$, and the radiation loss results in a gradual decrease of the norm. Nevertheless, the general predictions of the VA turn out to be correct for $a_1 \lesssim 0.05$: under the action of the management, oscillations of the soliton's parameters are regular for very small a_1, and become chaotic at larger a_1.

Typical examples of the soliton dynamics under the action of stronger management, with $a_1 \geq 0.1$ (and $\omega = 0.5$) are displayed in Fig. 15.2. A noteworthy observation, which could not be predicted by the single-soliton ansatz, is *splitting* of the pulse, which is observed, at $a_1 = 0.2$, in Fig. 15.2, while at other values of a_1, both smaller and larger than 0.2, the soliton remains centered around $n = 0$. Note that the splitting is similar to that revealed by direct simulations of the continuum NLS equation with a term accounting for periodic modulation of the linear dispersion (*dispersion management*), which was reported in [28]. A similar phenomenon was also observed in a discrete model with the finite-difference dispersion term subject to periodic modulation [29].

Results of the systematic numerical study of the evolution of solitons in Eq. (15.4) are summarized in Fig. 15.3 (for $a_1 \gtrsim 0.2$, the pulse may split into several moving splinters). The diagram shows that the actual critical value of management amplitude a_1, past which the soliton develops the instability (via the splitting) is *much higher* than the prediction of the chaotic dynamics threshold by the VA (which also eventually leads to the decay of the soliton, as the chaotic transient is followed by the asymptotic stage of the evolution with $\alpha(t) \to 0$, see above). Thus, the VA based on Eqs. (15.8) and (15.9) *underestimates* the effective stability of the discrete

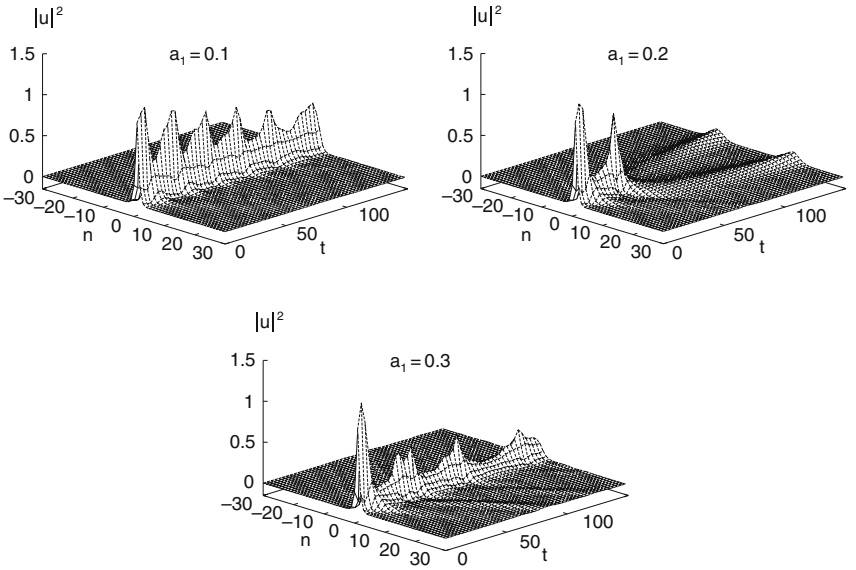

Fig. 15.2 Evolution of a discrete soliton with initial amplitude $A = 1$ in Eq. (15.4) with $\omega = 0.5$ and different values of the management amplitude, a_1. Reprinted from [22] with permission

solitons. This conclusion is explained by the fact that the radiation loss, that was ignored by the variational ansatz, plays a stabilizing role for the discrete solitons.

It is worth mentioning that the existence of a finite critical value of the modulation amplitude, past which the splitting occurs, and the fact that the actual stability area for solitons is larger than predicted by the VA are qualitatively similar to features found in the above-mentioned dispersion-management model based on the continuum NLS equation [28].

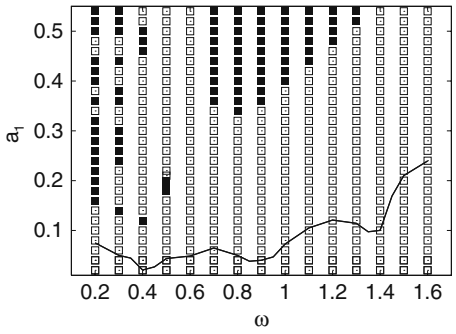

Fig. 15.3 The diagram of dynamical regimes in the plane of the FRM parameters, (ω, a_1), as produced by systematic simulations of Eq. (15.4) with $a_0 = 1$ and initial soliton's amplitude $A = 1$. *Open and solid squares* correspond to stable and splitting solitons, respectively. *The solid line* is the chaos-onset threshold predicted by the numerical solution of the variational equations (15.8) and (15.9). Reprinted from [22] with permission

15.3 Supporting Moving Solitons by Means of the "Management"

15.3.1 Analytical Approximation

In this part, we switch to the notation adopted in Eqs. (15.1) and (15.2), but again with $C \equiv 1$. The continuum limit (i.e., the ordinary NLS equation) suggests the following *ansatz* for a moving soliton [30]:

$$u(n,t) = A \exp\left[-b\,(n-\xi(t))^2 + i\phi(t) + \left(\frac{i}{2}\right)\dot{\xi}n - \frac{i}{4}\int \left(\dot{\xi}(t)\right)^2 dt\right], \quad (15.12)$$

where A, b, $\xi(t)$, and ϕ are, respectively, the amplitude, squared inverse width, central coordinate, and phase of the soliton. Accordingly, $\dot{\xi}$ is the soliton's velocity, $\dot{\xi}/2$ simultaneously being the wave number of the wave field which carries the moving soliton. Note the difference of this ansatz, which emulates the VA for the solitons in the continuum NLS equation [30], from the above-mentioned ansatz (15.6), that was adopted for the essentially discrete model. In the framework of the continuum NLS equation, the VA for the ordinary solitons yields

$$\dot{\phi} = 3b, \;\; A^2 = \frac{4\sqrt{2}b}{g} \quad (15.13)$$

(assuming that $g = c\text{const} > 0$), where b is treated as an arbitrary positive constant, i.e., intrinsic parameter of the soliton family.

Then, the ansatz (15.12) with zero velocity, $\dot{\xi} = 0$, may be substituted in the Hamiltonian corresponding to the DNLS equation (15.1),

$$H = \sum_{n=-\infty}^{+\infty}\left[2|u_n|^2 - \left(u_n^* u_{n+1} + u_n u_{n+1}^*\right) - \frac{g}{2}\,|u_n|^4\right]. \quad (15.14)$$

In this way, an effective potential of the soliton-lattice interaction is obtained in the form of a Fourier series, $H(\xi) = \sum_{m=0}^{\infty} H_m \cos(2\pi m\xi)$. In the case of a broad soliton, for which ansatz (15.12) is relevant, it is sufficient to keep only the lowest harmonic ($m = 1$) in this expression, which yields the respective PN (Peierls–Nabarro) potential, $U_{\rm PN}$. A straightforward calculation, using the Poisson summation formula, yields [23]

$$U_{\rm PN}(\xi) = \frac{1}{2}\sqrt{\frac{\pi}{b}}A^2 \exp\left(-\frac{\pi^2}{4b}\right)\left\{4\sqrt{2}\exp\left(-\frac{\pi^2}{4b}\right)\right.$$
$$\left.\left(1 + e^{-b/2}\right) - gA^2\sqrt{\frac{\pi}{b}}\right\}\cos(2\pi\xi). \quad (15.15)$$

If the relation between b and A^2, taken as for solitons in the continuum NLS equation, i.e., as per Eq. (15.13), is substituted into Eq. (15.15), the coefficient in front of $\cos(2\pi\xi)$, i.e., the amplitude of the PN potential, never vanishes. However, it may vanish if (15.12) is considered not as a soliton, but just as a pulse with independent amplitude and width, A and $1/\sqrt{b}$; then, the PN potential in Eq. (15.15) may vanish, under the following condition:

$$1+\exp\left(\frac{-b}{2}\right)=\left(\frac{gA^2}{4}\right)\sqrt{\frac{\pi}{2b}}\exp\left(\frac{\pi^2}{4b}\right). \tag{15.16}$$

The vanishing of the PN potential implies a possibility of unhindered motion of the soliton across the lattice.

For a broad soliton (small b), the PN potential barrier is exponentially small, hence, the soliton's kinetic energy may be much larger than the height of the potential barrier. Therefore, the velocity of the soliton moving through the potential (15.15) with period $L=1$ contains a constant (dc) part and a small ac correction to it, with frequency $2\pi\dot{\xi}_0/L\equiv 2\pi\dot{\xi}_0$ [31]: $\dot{\xi}(t)\approx\dot{\xi}_0+\dot{\xi}_1\cos\left(2\pi\dot{\xi}_0 t\right)$, $\dot{\xi}_1^2\ll\dot{\xi}_0^2$. Substituting this into condition (15.16), one can expand its left-hand side by using

$$\exp\left(\frac{-b}{2}\right)\cos\left(\frac{\dot{\xi}}{2}\right)\approx\exp\left(\frac{-b}{2}\right)\left[\cos\left(\frac{\dot{\xi}_0}{2}\right)-\frac{\dot{\xi}_1}{2}\sin\left(\frac{\dot{\xi}_0}{2}\right)\cos\left(2\pi\dot{\xi}_0 t\right)\right]. \tag{15.17}$$

Next, inserting the variable nonlinearity coefficient (15.2) into the right-hand side of Eq. (15.16), and equating the resulting expression to that (15.17), one concludes that $g_{\rm dc}$ and $g_{\rm ac}$ may be chosen so as to secure condition (15.16) to hold, provided that the average soliton's velocity takes the *resonant value*, $\dot{\xi}_0=\omega/2\pi$. More generally, due to anharmonic effects, one may expect the existence of a spectrum of the resonant velocities,

$$\dot{\xi}_0=(c_{\rm res})_N^{(M)}\equiv\frac{M\omega}{2\pi N} \tag{15.18}$$

with integers M and N.

Actually, an ac drive can support stable progressive motion of solitons at resonant velocities (15.18) (assuming that the spatial period is $L=1$), even in the presence of dissipation, in a broad class of systems. This effect was first predicted for discrete systems (of the Toda lattice and Frenkel–Kontorova types) in [32–35], and demonstrated experimentally in an LC electric transmission line [36]. Later, the same effect was predicted [37] and demonstrated experimentally [38] in long Josephson junctions with a spatially periodic inhomogeneity. However, a qualitative difference of the situation considered here is that we are now dealing with *nontopological solitons*, while the above-mentioned examples involved *kinks*, i.e., discrete or continuum solitons whose topological charge directly couples to the driving field.

15.3.2 Numerical Results

Numerical simulations of Eq. (15.1) (with $C = 1$) were performed in [23], setting $g_{\rm dc} = 1$ by means of the same rescaling which was used in the studies of the quiescent solitons. First, stationary solitons were found as solutions to the DNLS with $g_{\rm ac} = 0$, in the form of $u_n^{(0)}(t) = v_n \exp(-i\omega_0 t)$. Then, the FRM with $g_{\rm ac} > 0$ was switched on, and, simultaneously, the soliton was set in motion by giving it a *kick*, i.e., multiplying u_n by $\exp(iqn)$. Generic results in the plane of the ac-drive's parameters, $(\omega, g_{\rm ac})$, can be adequately represented by fixing $\omega_0 = -1$ and considering three values of the kick, $q = 0.25$, 0.5, and 1.

If $g_{\rm ac} = 0$, the kicked soliton does not start progressive motion if the thrust is relatively weak, $q \lesssim 0.7$. It remains pinned to the lattice, oscillating around an equilibrium position, which may be explained by the fact that the kinetic energy imparted to the soliton is smaller than the height of the PN potential barrier. Several types of dynamics can be observed with $g_{\rm ac} > 0$, depending on the modulation frequency ω and kick strength q. First, the soliton may remain pinned (generally, not at the initial position, but within a few sites from it, i.e., the soliton passes a short distance and comes to a halt, as shown in Fig. 15.4a). The next generic regime is that of *irregular motion*, as illustrated in Fig. 15.4b. A characteristic feature of that regime is that the soliton randomly changes the direction of motion several times, and the velocity remains very small in comparison with regimes of persistent motion, see below. The soliton's central coordinate, the evolution of which is presented in Fig. 15.4, is defined as $X = \sum_n n|u_n|^2/\mathcal{N}$, with the norm $\mathcal{N}$ calculated as per Eq. (15.3).

Under the action of strong modulation, the soliton can sometimes split into two pulses moving in opposite directions, see Fig. 15.5. This outcome is similar to that found for quiescent solitons, cf. Fig. 15.2b, although the splitting of the kicked soliton is strongly asymmetric (unlike the nearly symmetric splitting of the quiescent

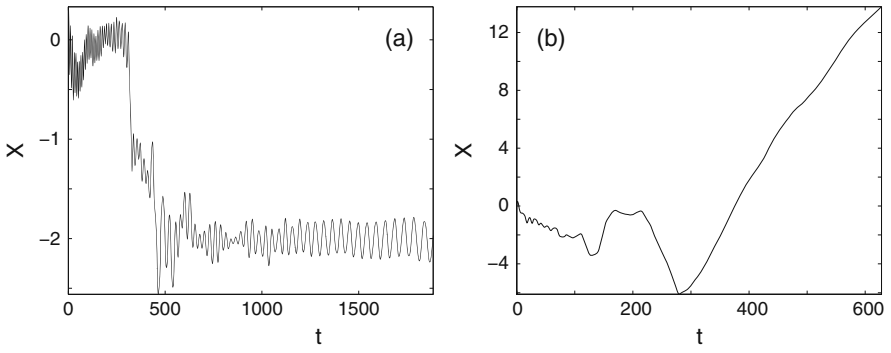

Fig. 15.4 The soliton's central position as a function of time, for typical cases in which the soliton remains pinned (**a**), at $g_{\rm ac} = 0.03$, or develops an irregular motion (**b**), at $g_{\rm ac} = 0.065$. In both cases, $\omega = 1$ and $q = 0.5$. Reprinted from [23] with permission

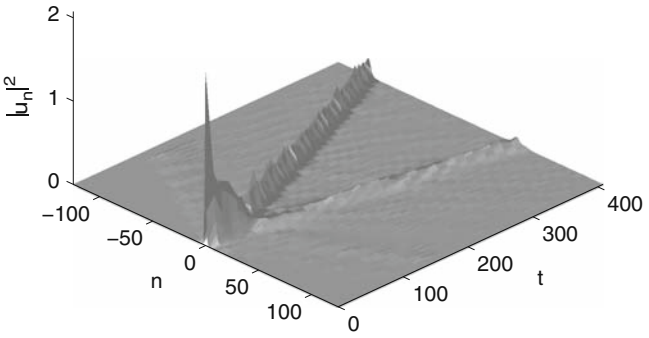

Fig. 15.5 An example of asymmetric splitting of the kicked soliton, for $q = 0.5$. The FRM parameters are $g_{ac} = 0.196$, $\omega = 0.5$. Reprinted from [23] with permission

solitons). The heavier splinter may move both forward and *backward*, relative to the initial kick.

In the case of moderately strong modulation, the moving soliton does not split. Numerical results demonstrate that, in some cases, it gradually decays into radiation, while in other cases it is completely stable, keeping all its norm, after an initial transient stage of the evolution, see examples in Figs. 15.6 and 15.7. To distinguish between the unstable and stable regimes, a particular criterion was adopted [23]. It categorizes as stable solitons those moving ones which keep $\geq 70\%$ of the initial norm in the course of indefinitely long evolution. For this purpose, very long evolution was implemented by allowing the soliton to circulate in the DNLS lattice with periodic boundary conditions.

Note that the soliton adjusting itself to the stable motion mode typically sheds off $\simeq 20\%$ of its initial norm. Although this conspicuous amount of the lattice radiation stays in the system with the periodic boundary conditions, it does not give rise to any appreciable perturbation of the established motion of the soliton. In fact, the latter observation provides for an additional essential evidence to the robustness of the moving soliton.

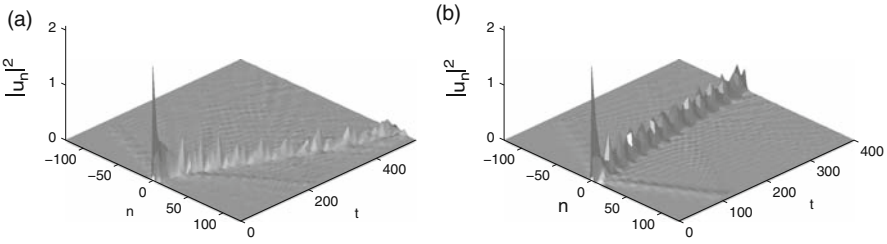

Fig. 15.6 Generic examples of the progressive motion of a decaying soliton in the straight (*forward*) direction (**a**), for $g_{ac} = 0.206$, $\omega = 0.5$, and in the reverse (*backward*) direction (**b**), for $g_{ac} = 0.170$, $\omega = 1$. In both cases, the solitons were set in motion by the application of the kick with $q = 0.5$. Reprinted from [23] with permission

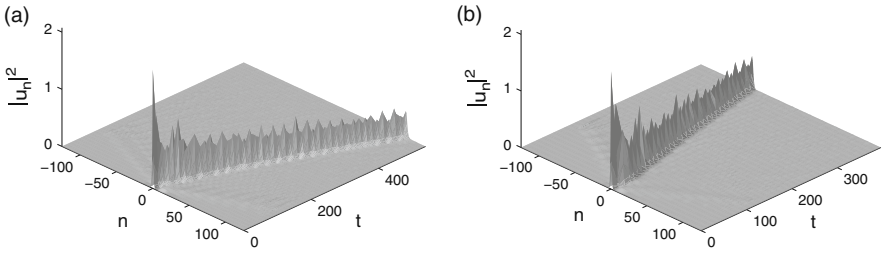

Fig. 15.7 Generic examples of the motion of propagating solitons in the straight direction (**a**), for $g_{\rm ac} = 0.132$, and in the reverse direction (**b**), for $g_{\rm ac} = 0.122$. In both cases, the modulation frequency is $\omega = 1$, and the kick is $q = 0.5$. Reprinted from [23] with permission

It is noteworthy too that, as seen in Figs. 15.6b and 15.7b, in both unstable and stable regimes the persistent motion of the soliton is possible in both the straight and reverse directions, relative to the initial thrust. In the latter case, the soliton starts the motion straight ahead, but very quickly bounces back. The difference from the regime of the irregular motion (cf. Fig. 15.4b) is that the direction of motion reverses only once, and the eventual velocity does not fall to very small values.

It is pertinent to compare the average velocity $\bar{c}$ of the persistent motion with the prediction given by Eq. (15.18). For example, in the cases displayed in Fig. 15.7a, b, the velocities found from the numerical data are $\bar{c}_a \approx 0.246$ and $\bar{c}_b \approx -0.155$, respectively. For $\omega = 1$, which is the corresponding modulation frequency, these values fit well to those predicted by Eq. (15.18) in the cases of, respectively, the second-order and fundamental resonance: $\bar{c}_b / (c_{\rm res})_1^{(1)} \approx 0.974$, $\bar{c}_a / (c_{\rm res})_3^{(2)} \approx 1.029$.

Lastly, results of systematic simulations of Eq. (15.1), which were performed, as said above, for the initial discrete soliton taken as a solution of the stationary version of the equation (for $g_{\rm ac} = 0$ and $g_{\rm dc} = 1$ in Eq. (15.2)) with $\omega = -1$, and for three values of the kick, $q = 0.25$, 0.5, and 1, are collected in Fig. 15.8 in the form of maps in the plane of the modulation parameters, $g_{\rm ac}$ and ω. The maps outline regions of the different dynamical regimes described above, as well as the distinction between regions of the straight and reverse progressive motion.

The examination of the maps shows that the increase of thrust q significantly affects the map, although quantitatively, rather than qualitatively. At all values of q, the irregular dynamics is, generally, changed by the stable progressive motion (straight or reverse) with the increase of the modulation amplitude and/or decrease of the frequency, which is quite natural. Further increase of the FRM strength, which implies the action of a strong perturbation, may lead to an instability, which indeed happens, in the form of onset of the gradual decay of the moving solitons. Finally, strong instability sets in, manifesting itself in the splitting of the soliton.

The reversal of the direction of the soliton's motion tends to happen parallel to the transition from stable moving solitons to decaying ones. For this reason, in most cases (but not always, see Fig. 15.7b) backward-moving solitons are decaying ones. Finally, a somewhat counterintuitive conclusion is that the increase of the initial

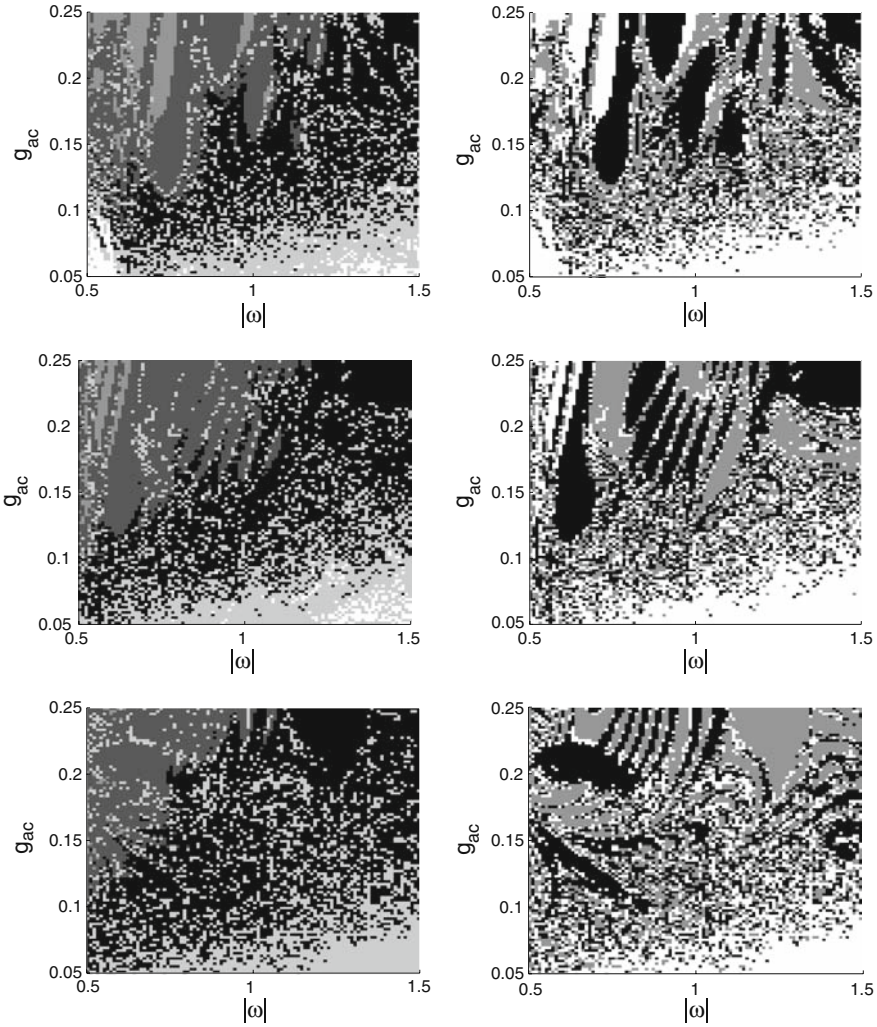

Fig. 15.8 Maps in the *left column* show areas in the plane of the FRM frequency and amplitude (ω, g_{ac}) which give rise to the following dynamical regimes. *White areas*: the soliton remains pinned; *bright gray*: irregular motion; *gray*: splitting; *dark gray*: regular motion with decay; *black*: *stable motion*. The maps in the *right column* additionally show the difference between the straight and reverse directions of the regular motion (marked by *dark gray and black*), relative to the direction of the initial thrust. Regular-motion regimes for both decaying and stable solitons are included in the *right-hand panels*. *Top row*: $q = 0.25$; *middle row*: $q = 0.5$; *bottom row*: $q = 1$. Reprinted from [23] with permission

thrust leads to overall *stabilization* of the soliton, making the decay and splitting zones smaller.

Collisions between solitons moving with opposite velocities (generated by thrusts $\pm q$ applied to two far separated quiescent solitons) were studied too, using the

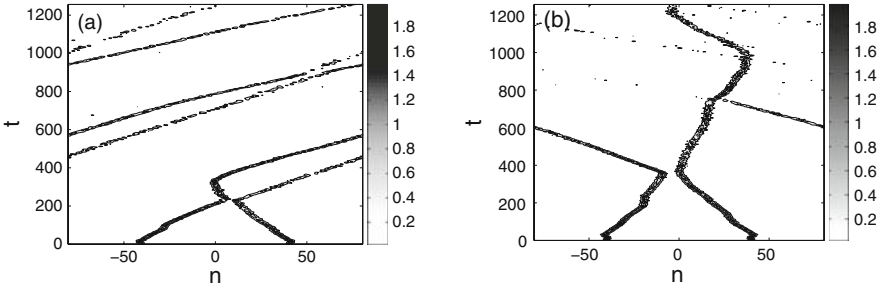

Fig. 15.9 Two generic outcomes of collisions between identical solitons moving in opposite directions, in the lattice with periodic boundary conditions. The parameters are $g_{\rm ac} = 0.132$, $\omega = 1$, $q = 0.5$ (**a**) and $g_{\rm ac} = 0.122$, $\omega = 1$, $q = 0.5$ (**b**). Note the presence of multiple collisions in panel (b). Reprinted from [23] with permission

lattice with periodic boundary conditions (which allow repeated collisions). Two different types of the interaction can be identified, see typical examples in Fig. 15.9. In the case shown in Fig. 15.9a, the solitons bounce back from each other almost elastically. Afterward, one of them spontaneously reverses the direction of motion, due to its interaction with the lattice. Eventually, a pair of virtually noninteracting solitons traveling indefinitely long in the same direction is observed.

In the other case, shown in Fig. 15.9b, the solitons also bounce after the first collision; however, in this case the collision is inelastic, resulting in transfer of mass from one soliton to the other. Repeated collisions (due to the periodicity of the lattice) lead to additional such transfer, and the weaker soliton disappears eventually. In contrast to what is known about collisions between moving solitons in the ordinary DNLS equation (with constant coefficients) [17], merger of colliding solitons into a single standing one was not observed under the action of the management (FRM).

15.4 Conclusion and Future Challenges

The use of the nonlinearity management may provide for a powerful tool for the control of the dynamics of standing and moving discrete solitons. In the present chapter, these possibilities were outlined for the 1D settings. The action of a similar "management" on two-dimensional (2D) discrete fundamental and vortex solitons, which, in terms of the BEC, may also be readily implemented by means of the FRM, has not been investigated as yet.

The stability limits of 2D solitons, against periodic modulation of the strength of the potential, in the continuum Gross–Pitaevskii equation have been recently studied. The considered model includes the self-attractive cubic nonlinearity and a quasi-1D [39] or full 2D [40] OL potential. In fact, the respective solitons may be considered as quasi-discrete ones; accordingly, in terms of discrete equation (15.1), this "lattice management" corresponds to making the lattice coupling constant a periodic function of time, $C = C(t)$.

As concerns the application of the nonlinearity management to 2D lattice solitons, challenging issues are a possibility of the generation of moving 2D lattice solitons, as well as the control of vortex solitons and bound states of fundamental solitons by means of this technique. These applications may pertain to both isotropic and anisotropic lattices.

A similar management technique may be applied to waveguide arrays or photonic crystals made of photorefractive materials. These systems can be described by DNLS equations with a saturable nonlinearity.

References

1. Kevrekidis, P.G., Rasmussen, K.Ø., Bishop, A.R.: Int. J. Mod. Phys. B **15**, 2833 (2001) 277
2. Christodoulides, D.N., Joseph, R.I.: Opt. Lett. **13**, 794 (1988) 277
3. Peschel, U., Morandotti, R., Arnold, J.M., Aitchison, J.S., Eisenberg, H.S., Silberberg, Y., Pertsch, T., Lederer, F.: J. Opt. Soc. Am. B **19**, 2637 (2002) 277
4. Eisenberg, H.S., Morandotti, R., Silberberg, Y., Arnold, J.M., Pennelli, G., Aitchison, J.S.: J. Opt. Soc. Am. B **19**, 2938 (2002) 277
5. Trombettoni, A., Smerzi, A.: Phys. Rev. Lett. **86**, 2353 (2001) 277
6. Abdullaev, F.Kh., Baizakov, B.B., Darmanyan, S.A., Konotop, V.V., Salerno, M.: Phys. Rev. A **64**, 043606 (2001) 277
7. Alfimov, G.L., Kevrekidis, P.G., Konotop, V.V., Salerno, M.: Phys. Rev. E **66**, 046608 (2002) 277
8. Smerzi, A., Trombettoni, A.: Phys. Rev. A **68**, 023613 (2003) 277
9. Smerzi, A., Trombettoni, A.: Chaos **13**, 766 (2003) 277
10. Efremidis, N.K., Christodoulides, D.N.: Phys. Rev. A **67**, 063608 (2003) 277
11. Porter, M.A., Carretero-González, R., Kevrekidis, P.G., Malomed, B.A.: Chaos **15**, 015115 (2005) 277
12. Malomed, B. Weinstein, M.I.: Phys. Lett. A **220**, 91 (1996) 277, 279
13. Malomed, B.A.: In Progress in Optics. Wolf, E. (ed.), vol. 43, p. 71. North Holland, Amsterdam (2002) 277, 279
14. Duncan, D.B., Eilbeck, J.C., Feddersen, H., Wattis, J.A.D.: Physica D **68**, 1 (1993) 277
15. Flach, S., Zolotaryuk, Y. Kladko, K.: Phys. Rev. E **59**, 6105 (1999) 277
16. Ablowitz, M.J., Musslimani, Z.H., Biondini, G.: Phys. Rev. E **65**, 026602 (2002) 277
17. Papacharalampous, I.E., Kevrekidis, P.G., Malomed, B.A., Frantzeskakis, D.J.: Phys. Rev. E **68**, 046604 (2003) 277, 289
18. Kivshar, Yu.S., Malomed, B.A.: Rev. Mod. Phys. **61**, 763 (1989) 277
19. Kivshar, Y.S., Campbell, D.K.: Phys. Rev. E **48**, 3077 (1993) 277
20. Brizhik, L., Eremko, A., Cruzeiro-Hansson, L., Olkhovska,Y.: Phys. Rev. B **61**, 1129 (2000) 277
21. Kevrekidis, P.G., Kevrekidis, I.G., Bishop, A.R., Titi, E.S.: Phys. Rev. E **65**, 046613 (2002) 277
22. Abdullaev, F.Kh., Tsoy, E.N., Malomed, B.A., Kraenkel, R.A.: Phys. Rev. A **68**, 053606 (2003) 278, 279, 280, 281, 282
23. Cuevas, J., Malomed, B.A., Kevrekidis, P.G.: Phys. Rev. E **71**, 066614 (2005) 278, 283, 285, 286, 287, 288
24. Donley, E.A., Claussen, N.R., Thompson, S.T., Wieman, C.E.: Nature, **417**, 529 (2002) 278
25. Kevrekidis, P.G., Theocharis, G., Frantzeskakis, D.J., Malomed, B.A.: Phys. Rev. Lett. **90**, 230401 (2003) 278
26. Malomed, B.A.: Soliton Management in Periodic Systems. Springer, New York (2006) 278
27. Ott, E.: Chaos in Dynamical Systems. Cambridge University Press, Cambridge (1993) 280
28. Grimshaw, R., He, J., Malomed, B.A.: Phys. Scripta **53**, 385 (1996) 281, 282
29. Peschel, U., Lederer, F.: J. Opt. Soc. Am. B **19**, 544 (2002) 281
30. Anderson, D.: Phys. Rev. A **27**, 3135 (1983) 283
31. Peyrard, M., Kruskal, M.D.: Physica D **14**, 88 (1984) 284

32. Malomed, B.A.: Phys. Rev. A **45**, 4097 (1992) 284
33. Bonilla, L.L., Malomed, B.A.: Phys. Rev. B **43**, 11539 (1991) 284
34. Kuusela, T., Hietarinta, J., Malomed, B.A.: J. Phys. A **26**, L21 (1993) 284
35. Filatrella, G., Malomed, B.A.: J. Phys. Cond. Matt. **11**, 7103 (1999) 284
36. Kuusela, T.: Chaos Sol. Fract. **5**, 2419 (1995) 284
37. Filatrella, G., Malomed, B.A., Parmentier, R.D.: Phys. Lett. A **198**, 43 (1995) 284
38. Ustinov, A.V., Malomed, B.A.: Phys. Rev. B **64**, 020302 (2001) 284
39. Mayteevarunyoo, T., Malomed, B.A., Krairiksh, M.: Phys. Rev. A **76**, 053612 (2007) 289
40. Burlak, G., Malomed, B.A.: Phys. Rev. A **77**, 053606 (2008) 289